Peak boundary selection in photopeak integration by the method of Covell

ARTICLE *in* ANALYTICAL CHEMISTRY · DECEMBER 1972

Impact Factor: 5.64 · DOI: 10.1021/ac60322a006

2 AUTHORS, INCLUDING:

Kaj Heydorn

130 PUBLICATIONS **1,132** CITATIONS

SEE PROFILE

Peak boundary selection in photopeak integration by the method of Covell

Kaj. Heydorn, and Witold. Lada

Anal. Chem., **1972**, 44 (14), 2313-2317 • DOI: 10.1021/ac60322a006

Peak Boundary Selection in Photopeak Integration by the Method of Covell

Kaj Heydorn and Witold Łada[1]

Isotope Division, Danish Atomic Energy Commission Research Establishment Risö, DK 4000, Roskilde, Denmark

The relationship between the precision of photopeak integration by the method of Covell and the number of channels used in the calculation has been studied mathematically as well as experimentally. A Gaussian peak superimposed on a straight line is used in the mathematical development, and a functional relationship between relative peak height, peak width, and integration width was established for which maximum relative precision would be achieved. A graphical representation of this relationship permits direct application for practical purposes. For the experimental investigation series of spectra of precisely known admixtures of ^{54}Mn to ^{59}Fe were generated, using the NaI(Tl) scintillation detector as well as the Ge(Li) semiconductor detector. Excellent agreement with predicted points of maximum precision was observed, and a calculated optimum integration half-width of 0.91 × full width at half maximum for small relative peak heights was confirmed.

IN THE DETERMINATION of elements by neutron activation analysis the quantitative evaluation of digital γ-spectra from multi-channel analyzers is of fundamental significance. Although a great variety of methods are used for this purpose (*1*), photopeak integration appears to win most general acceptance (*2*), and the classical methods for the determination of peak area have been supplemented with more involved calculations (*3*). In spite of the improved precision that can be achieved in this way, the original method of Covell (*4*) is still the most widely used method for photopeak integration.

The method yields accurate results, provided the peak is free from interference from extraneous γ-rays, and its base may be accurately represented by a straight line—or is accurately known from a reference spectrum. Calculation of peak areas and their standard deviations is easily done manually or with a simple desk calculator, which facilitates the implementation of the method in the analytical laboratory.

The precision of Covell's method depends on the number of channels used in the calculation, and particularly, when no peak is detected, the choice of boundary channels giving the lowest upper limit at a particular level of confidence assumes importance.

MATHEMATICAL DEVELOPMENT

Digital Formulation. Let a γ-spectrum recorded with a detector of resolution R, connected to a multi-channel analyzer at a gain g, contain a photopeak of energy E and a total peak area P standing on a sloping continuum.

The pulse-height distribution $N(i)$ is illustrated in Figure 1, where the peak is centered in channel $I = E/g$ with a peak height a and a full width at half maximum $w = R \times I$.

[1] Present address, Institute of Nuclear Research, Swierk, Poland.

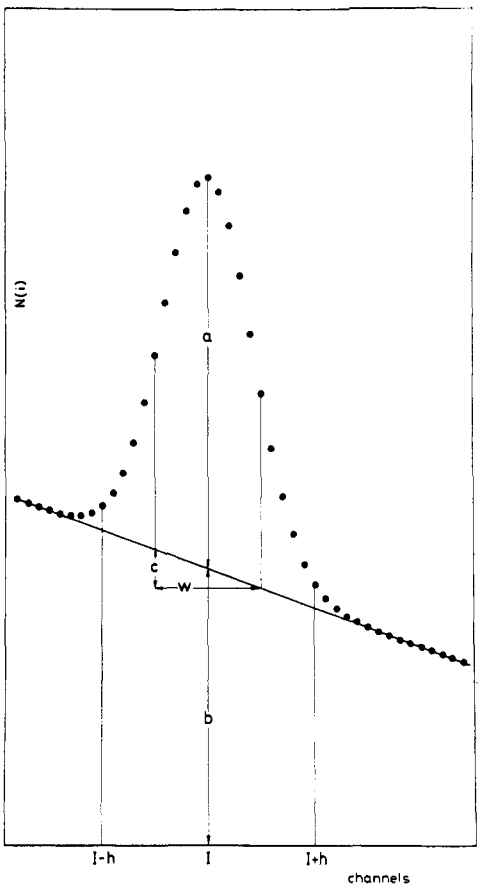

Figure 1. Gaussian peak on a linear continuum

The height of the continuum in channel I is b and its slope $\alpha = -c/w$ where $b/a = \beta$ and $c/a = \gamma$.

A given source and detector combination fixes E, R, β, and γ, while P is determined by counting time, and w and I are determined by the gain of the system.

Calculation of the peak area by the method of Covell, using h channels on either side of the peak channel gives

$$A = \sum_{I-h+1}^{I+h-1} N(i) - (2h - 1) \times {}^1/_2 \times [N(I - h) + N(I + h)] \quad (1)$$

Assuming absence of correlation between different channels in the spectrum (*5*), the corresponding variance may be calculated as

$$V = \sum_{I-h+1}^{I+h-1} N(i) + \left(\frac{2h - 1}{2}\right)^2 \times [N(I - h) + N(I + h)]$$

$$= A + \left(\frac{2h - 1}{2}\right) \times \left(\frac{2h + 1}{2}\right) \times [N(I - h) + N(I + h)] \quad (2)$$

(1) H. P. Yule, "Modern Trends in Activation Analysis," *Nat. Bur. Stand. (U.S.), Spec. Publ.*, **312**, 1969, p 1155.
(2) H. P. Yule, "Activation Analysis in Geochemistry and Cosmochemistry," Universitetsforlaget, Oslo, 1971, p 145.
(3) P. A. Baedecker, ANAL. CHEM., **43**, 405 (1971).
(4) D. F. Covell, *ibid.*, **31**, 1785 (1959).
(5) N. D. Eckhoff, *Nucl. Instrum. Methods*, **68**, 93 (1969).

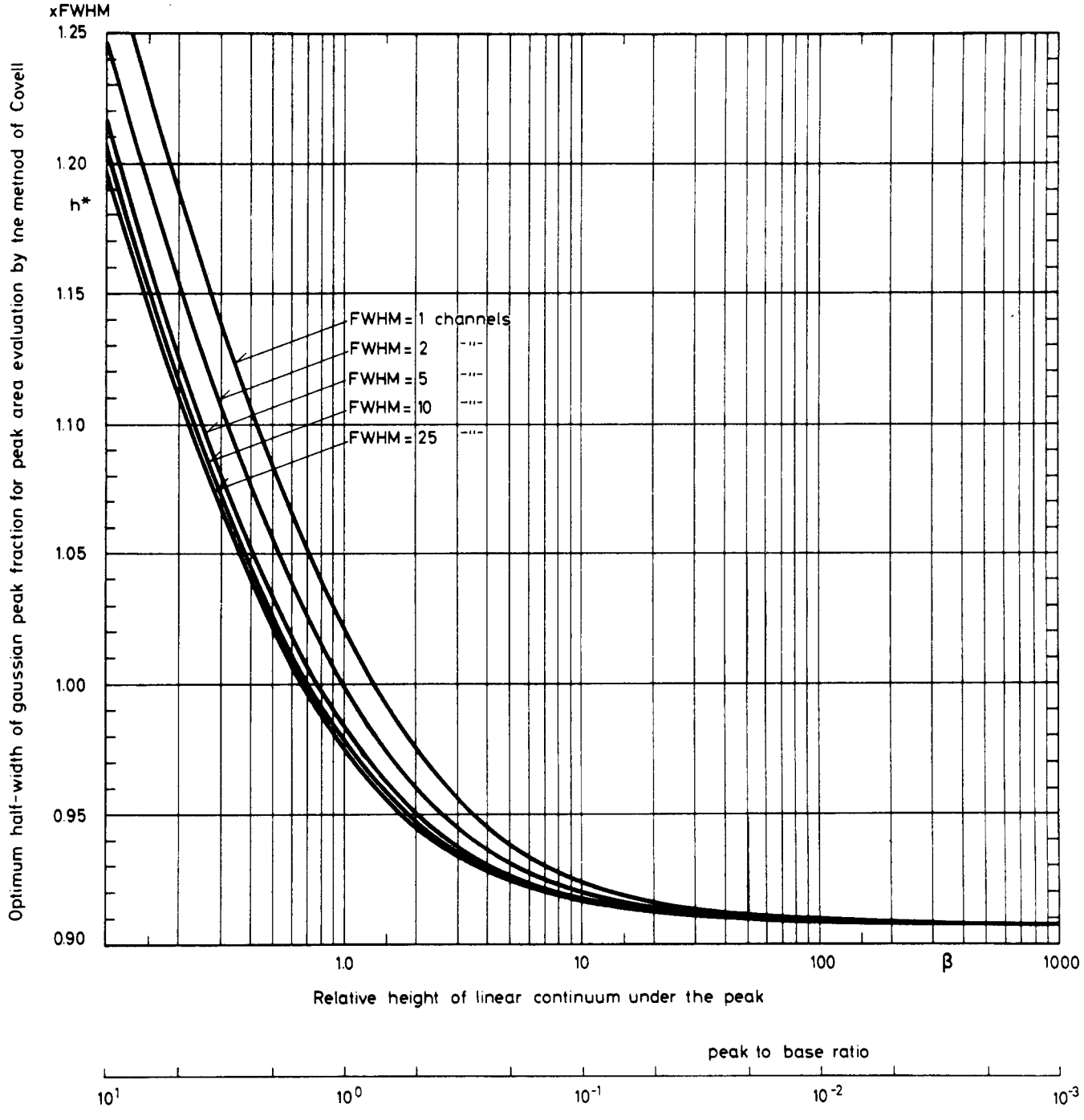

Figure 2. Optimum half-width of Gaussian peak fraction for peak area evaluation by the method of Covell as a function of height of linear continuum under the peak for selected values of full width at half maximum

Maximum relative precision in peak area evaluation by the method of Covell is achieved, when h is selected so that $A/\sqrt{V}$ is maximized.

Analog Representation. The pulse-height distribution shown in Figure 1 can be approximated by a Gaussian curve superimposed on a straight line, expressed as

$$y = \frac{P}{\sigma\sqrt{2\pi}} e^{-1/2\left(\frac{x-x_o}{\sigma}\right)^2} + y_o + \alpha(x - x_o) \qquad (3)$$

where

$$\sigma = \frac{w}{2\sqrt{2\ln 2}} \text{ and } (x_o, y_o) = (I, b)$$

Since

$$a = \frac{P}{\sigma\sqrt{2\pi}} \text{ and } \alpha = -\frac{c}{w}$$

the introduction of

$$t = \frac{x - x_o}{\sigma} \text{ and } \alpha^* = \frac{\gamma}{2\sqrt{2\ln 2}}$$

transforms Expression 3 into

$$y = a(e^{-t^2/2} + \beta - \alpha^* t) \qquad (4)$$

Calculation of the peak area by

$$A^* = \int_{x_o-h}^{x_o+h} y\,dx - 2h \times {}^1/_2 \times (y_{x_o-h} + y_{x_o+h}) \qquad (5)$$

is strictly equivalent to the calculation by the method of Covell in Expression 1, and the corresponding variance given in Equation 2 is equivalent to

$$V^* = A^* + h^2 \times (y_{x_0-h} + y_{x_0+h}) \tag{6}$$

provided $4h^2 \gg 1$.

Determination of h^* corresponding to

$$\text{maximum of the function } A^*/\sqrt{V^*} \tag{7}$$

is therefore equivalent to achieving maximum relative precision by the method of Covell.

Determination of Optimum Half-Width. The integration half-width h^* is calculated by maximizing Equation 7 with respect to T, where $h = \sigma \times T$

$$\delta\left(\frac{A^*}{\sqrt{V^*}}\right)\Big/\delta T = \frac{V^* \times \delta A^*/\delta T - {}^1/_2 A^* \times \delta V^*/\delta T}{V^*\sqrt{V^*}},$$

which equals zero for

$$\frac{\delta V^*/\delta T}{\delta A^*/\delta T} = 2\,\frac{V^*}{A^*} \tag{8}$$

With T as the independent variable, Equation 5 is transformed into

$$A^* = \frac{P}{\sqrt{2\pi}}\left[\int_{-T}^{T} (e^{-t^2/2} + \beta - \alpha^* t)dt - T(2e^{-T^2/2} + 2\beta)\right]$$

$$= \frac{2P}{\sqrt{2\pi}}\left[\int_0^T e^{-t^2/2}\,dt - T \times e^{-T^2/2}\right] \tag{9}$$

and Equation 6 becomes

$$V^* = \frac{2P}{\sqrt{2\pi}} \times \left[\int_0^T e^{-t^2/2}\,dt - T \times e^{-T^2/2} + \sigma T^2 (e^{-T^2/2} + \beta)\right] \tag{10}$$

By means of the auxiliary variables

$$F = \frac{\int_0^T e^{-t^2/2}\,dt}{T \times e^{-T^2/2}} \text{ and } B = \frac{\beta}{e^{-T^2/2}}$$

and the derivatives of Equations 9 and 10

$$\delta A^*/\delta T = \frac{2P}{\sqrt{2\pi}} \times T^2 \times e^{-T^2/2} \tag{11}$$

$$\delta V^*/\delta T = \frac{2P}{\sqrt{2\pi}} \times T \times e^{-T^2/2}[T(1 - \sigma T) + 2\sigma(1 + B)] \tag{12}$$

Equation 8 can be expressed as

$$\frac{T(1 - \sigma T) + 2\sigma(1 + B)}{T} = 2\,\frac{F - 1 + \sigma T(1 + B)}{F - 1} \tag{13}$$

Separation of B gives

$$1 + B = \frac{1 + \sigma T}{2\sigma} \times \frac{(F - 1) \times T}{F - 1 - T^2} \tag{14}$$

Equation 14 shows that the optimum value $h^* = \sigma \times T$ is independent of P, the absolute number of counts in the photopeak, and of α, the slope of the continuum.

It is determined solely by the relative height of the continuum, β, and the full width at half maximum $w = 2.355 \times \sigma$.

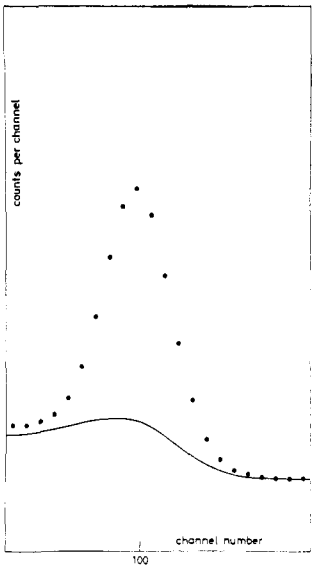

Figure 3. Photopeak of ^{54}Mn on top of ^{59}Fe Compton distribution recorded with a NaI(Tl) scintillation detector

Discussion. Equation 14 determines the relationship between the optimum half-width h^* and the parameters β and w, but is not applicable for explicit calculation of h^*.

The range of values assumed by β is virtually unlimited, while w in practice is restricted to the interval [1;25]; a graphical representation of h^* as a function of β for selected values of w is therefore a convenient solution of Equation 14.

Interpolation between discrete values of w then becomes necessary, and this is greatly facilitated by expressing h^* in units of w.

In Figure 2, the optimum half-width $\dfrac{T}{2\sqrt{2 \ln 2}} = \dfrac{h^*}{w}$ in units of full width at half maximum is shown as a function of β in the range [0.1; 1000] for selected values of w. The β scale is supplemented by a scale of $1/\beta$ showing the corresponding peak-to-base ratios.

For $\beta \to 0$, the optimum half-width $h^* \to \infty$ for all w, but more interesting is it that for $\beta \to \infty$, the value of h^*/w becomes independent of w. This limiting value is determined by the denominator in Equation 14.

$$F - 1 - T^2 = 0 \tag{15}$$

which is satisfied for $h^* = 0.90758\,w$.

The maximum signal to noise ratio is found for $F = 2$ with $h = 0.59452\,w$. This concept refers to the situation where the mean value of the base is known with infinite precision; this is not assumed in the application of the Covell method, which therefore has its optimum at a greater integration width.

The value of $0.90758\,w$ is of importance when no peak has been detected, because it results in the lowest upper limit at a given level of confidence.

EXPERIMENTAL

In the mathematical development, various assumptions are made that are only partially fulfilled in actual experiments.

The Gaussian shape of the photopeak is not maintained in the region $h > 0.9\,w$, where the optimum precision is expected;

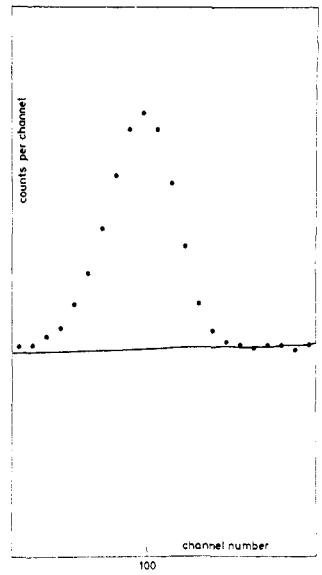

Figure 4. Photopeak of ^{54}Mn on top of ^{59}Fe Compton distribution recorded with a Ge(Li) semiconductor detector

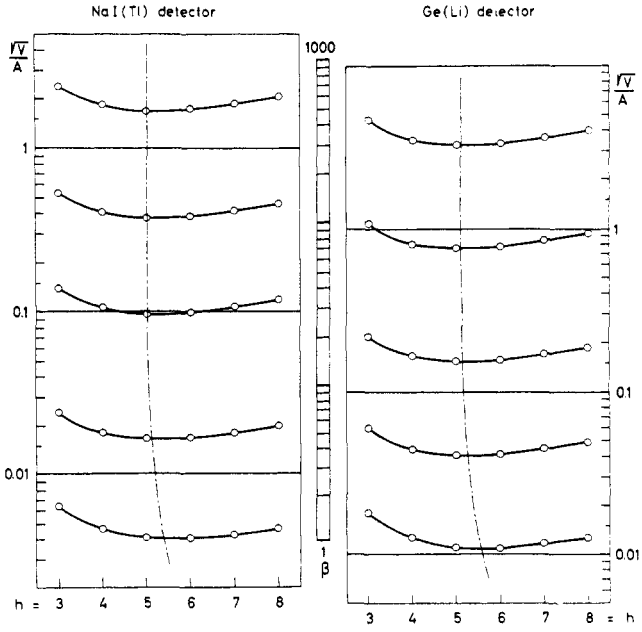

Figure 5. Experimental relative standard deviation as a function of the number of channels from the peak channel for different relative heights of plateau β

To the left are results from the NaI(Tl) scintillation detector, to the right those from the Ge(Li) semiconductor detector

particularly the low-energy side of the peak exhibits significant deviations from the Gaussian.

A rectilinear base has been assumed, but possible deviations from this in a real spectrum have not been taken into account.

On the other hand the condition $4\,h^2 \gg 1$ will usually be fulfilled in practice because full widths at half maximum of less than 5 channels are rarely used.

In the experimental tests the slightly different shapes of photopeaks produced by a NaI(Tl) scintillation detector and a Ge(Li) semiconductor detector were taken into account. By using combined sources of ^{54}Mn and ^{59}Fe, two different types of base are produced at the same time, as shown in Figures 3 and 4. In the spectrum from the scintillation detector, the 835 keV photopeak from ^{54}Mn is standing on the Compton shoulder from the 1099 keV photopeak of ^{59}Fe, while in the spectrum from the semiconductor detector, the base is a practically flat Compton continuum.

Table I. Experimental Conditions

	NaI(Tl) scintillation detector	Ge(Li) semiconductor detector
^{59}Fe source strength	6.4 μCi	3.2 μCi
^{54}Mn source strength	5.6 μCi	4.2 μCi
Source–detector distance	82 mm	32 mm
Dead-time	12%	16%
Gain	12.4 keV/channel	0.61 keV/channel
FWHM of photopeak	5.5 channels	5.6 channels
Stability of peak position	Better than 0.05 channel	Better than 0.1 channel

Procedure. Spectra corresponding to precisely known mixtures of ^{59}Fe and ^{54}Mn were recorded with a Nuclear Data 3300 System 4096-channel analyzer connected to a Harshaw 3-in. × 3-in. NaI(Tl) scintillation detector, alternatively a Canberra coaxial Ge(Li) semiconductor detector.

Counting took place at a gain, yielding a ^{54}Mn photopeak with a full width at half maximum of about 5.5 channels, and with a zero intercept centering the 835 keV phototop in channel 100.

A pure ^{59}Fe source in the form of 1 ml of aqueous solution in a half-dram polyvial was counted, until well over 10^4 counts per channel were recorded in the vicinity of channel 100. After removal of the source, background subtraction was carried out, and a 1-ml aqueous solution of pure ^{54}Mn took the place of the ^{59}Fe source.

A series of spectra were now produced by counting ^{54}Mn on top of the ^{59}Fe spectrum, and finally a pure ^{54}Mn spectrum was recorded as a reference.

The precise contribution of ^{54}Mn to the mixed spectra relative to the reference is here monitored by the internal reference oscillator of the multi-channel analyzer, which is counted in the first channel of the spectrum.

A specification of experimental conditions for the two sets of measurements is given in Table I. Sources of ^{59}Fe and ^{54}Mn were matched so as to produce the same per cent dead-time, when placed in the same counting position.

No variation in gain and zero intercept could be detected during the experiments, and pile-up distortion was reduced to insignificance by a rejector. The composite spectra therefore represent the shapes of spectra obtained from mixtures of ^{59}Fe and ^{54}Mn at low count rates.

RESULTS

Experimental results for the relative precision obtained by the method of Covell, with mixtures of ^{59}Fe and ^{54}Mn are presented in Figure 5, where $\sqrt{V}/A$ is plotted as a function of h for different ^{54}Mn to ^{59}Fe ratios.

Spectra corresponding to activity ratios between 10^{-1} and 2×10^{-4} were chosen for the scintillation detector and between 10^{-4} and 3×10^{-2} for the semiconductor detector.

Superimposed on these plots are graphs of h^* as a function of β determined from Figure 2 using $w = FWHM$ from Table I.

Since experimental values of $\sqrt{V}/A$ can be available only for integer values of h, and the truncated value of h^* was 5 for all spectra, the β-scale was linked to the logarithmic scales of $\sqrt{V}/A$ for $h = 5$. Considering the small variation of $\sqrt{V}/A$ in the vicinity of a minimum, the graphs are very good approxi-

mations to the relation between h^* and the expected minimum values of $\sqrt{V^*}/A^*$.

Activity ratios for $\beta = 1$ are 0.11 for the scintillation detector and 0.03 for the semiconductor; for large β the $\sqrt{V}/A$ becomes proportional to β, and the β-scale becomes truly logarithmic. The displacement of the logarithmic scales for the scintillation detector and the semiconductor detector reflects the difference in the absolute number of counts per channel accumulated during the measurement of the respective ^{59}Fe sources.

The agreement between calculation and experiment is illustrated by the passage of the h^* *vs.* β graph through the minimum of curves drawn through the experimental points for $\sqrt{V}/A$ for values of h from 3 to 8.

DISCUSSION

In spite of deviations from the Gaussian shape, particularly for the photopeak in the Ge(Li) detector spectrum, and in spite of a pronounced nonlinear shape of the base in the scintillation detector spectrum, the mathematical calculation of the point of maximum precision has been verified under experimental conditions.

This means that the graphs in Figure 2 can be used to predict the best boundaries for peak area calculation by the method of Covell, also for spectra where no definite photopeak is observed. Selection of boundaries nearest to $I \pm h^*$ will in many cases be tantamount to choosing 1 full width at half maximum to either side of the peak channel.

The observed decrease in precision with increasing deviation from the optimum half-width h^* is largely independent of the relative peak height, and it is quite similar for the two different detectors used. The proper choice of h is most important for measurements near the limit of detection with Ge(Li) semiconductor detectors, where long counting times are involved; the per cent increase in counting time equivalent to a deviation of h from h^* is shown in Figure 6, which represents the generalized shape of the curves for the Ge(Li) detector in Figure 5.

A comparison has been made with the method of *total peak area* calculation, using peak boundary selection by the criteria introduced by Yule (*6*). The accuracy of this method is less influenced by variations in gain and resolution (*7*), but rather more by base-line curvature, because of the larger number of channels involved.

Calculations of total peak areas were made by using a 5-point smoothing of data, and it was found that in spite of the improvement in precision resulting from the use of smoothed boundary values, the relative standard deviation exceeded that of the Covell method in all cases.

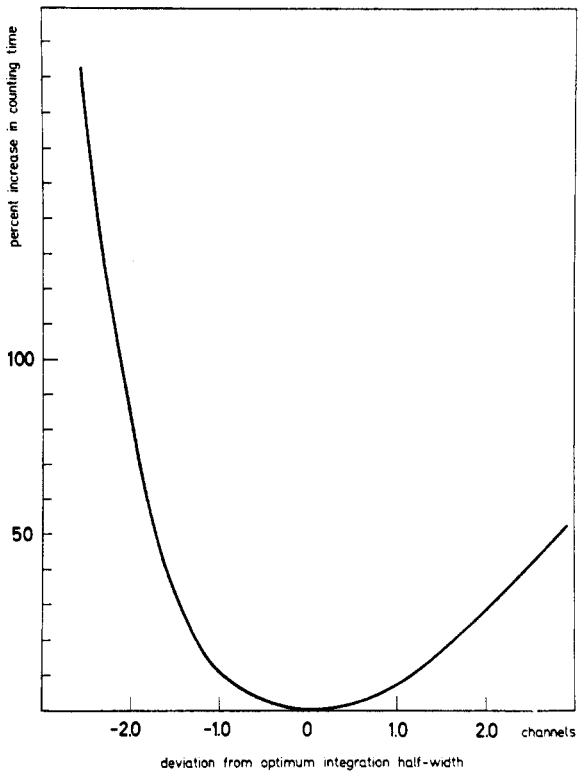

Figure 6. Increase in counting time required to compensate for loss of precision caused by deviation from optimum integration half-width for the Ge(Li) detector

For large relative peak heights the difference was negligible, but for small peaks where the boundaries are determined solely by the shape of the Compton continuum, the equivalent increase in counting time was 40% for the Ge(Li) detector and 140% for the scintillation detector.

The use of amplifiers with pole-zero correction together with base-line restoration and pulse pile-up rejection has greatly reduced shifts and resolution changes in connection with semiconductor detectors. For such counting systems, the classical method of Covell using optimum boundary channels appears preferable to the total peak area method with respect to precision as well as accuracy, when relative peak heights are less than unity.

RECEIVED for review March 1, 1972. Accepted July 6, 1972. One of the authors (WL) is grateful to the International Atomic Energy Agency for a fellowship.

(6) H. P. Yule, ANAL. CHEM., **38**, 103 (1966).
(7) *Ibid.*, **40**, 1480 (1968).